FULL ARTICLE

Stereotaxic endoscopy for the ocular imaging of awake, freely moving animal models

Bjorn Paulson[1] | Sangwook Lee[2] | Miyeon Jue[1] | Kyungsung Lee[1] |
Sanghwa Lee[1] | Guk Bae Kim[3] | Youngjin Moon[1,2] | Joo Yong Lee[4] |
Namkug Kim[2]* | Jun Ki Kim[1,2]* ⓘ

[1]Biomedical Engineering Research Center, Asan Institute for Life Science, Asan Medical Center, Seoul, South Korea

[2]Department of Convergence Medicine, College of Medicine, University of Ulsan, Seoul, South Korea

[3]ANYMEDI Inc., Seoul, South Korea

[4]Department of Ophthalmology, College of Medicine, University of Ulsan, Asan Medical Center, Seoul, South Korea

*Correspondence
Namkug Kim, Department of Convergence Medicine, College of Medicine, University of Ulsan, 88, Olympic-ro 43-gil, Songpa-gu, Seoul 05505, South Korea.
Email: namkugkim@gmail.com

Jun Ki Kim, Biomedical Engineering Research Center, Asan Institute for Life Science, Asan Medical Center, 88, Olympic-ro 43-gil, Songpa-gu, Seoul 05505, South Korea.
Email: kim@amc.seoul.kr

Abstract

Stereotaxic instruments are increasingly used in research animals for the study of disease, but typically require restraints and anesthetic procedures. A stereotaxic head mount that enables imaging of the anterior chamber of the eye in alert and freely mobile mice is presented in this study. The head mount is fitted based on computed tomography scans and manufactured using 3D printing. The system is placed noninvasively using temporal mount bars and a snout mount, without breaking the skin or risking suffocation, while an instrument channel stabilizes the ocular probes. With a flexible micro-endoscopic probe and a confocal scanning laser microscopy system, <20 μm resolution is achieved in vivo with a field of view of nearly 1 mm. Discomfort is minimal, and further adaptations for minimally invasive neuroscience, optogenetics and auditory studies are possible.

Stereotaxic head mount. In vivo iris fluorescent angiography
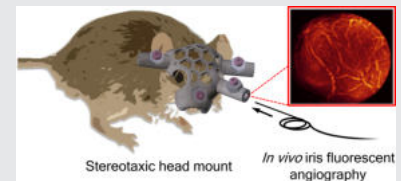
KEYWORDS

additive manufacturing, animal experimentation, endoscopy, minimally invasive, ophthalmology, stereotaxic

1 | INTRODUCTION

Mice are increasingly used as models in neuroscience,[1–3] optogenetics,[4, 5] vision[6–8] and diabetes[9, 10] research studies due to the relatively low cost of animal care and the availability of either wild-type mouse lines or transgenic mouse models of specific human diseases. Advances in mouse neuroscience have been enabled by the development of stereotaxic (sometimes called

stereotactic) coordinates for the mouse brain,[11] which identify the positions of key regions in the brain relative to reference points such as the lambda and the bregma. These coordinates are used in tandem with standardized stereotaxic surgical techniques—most commonly clamps and general anesthesia procedures—for the precise placement of cannulae[12] and electrodes[13] in the mouse brain. While these standard stereotaxic restraining platforms[14] can be used for monitoring neuronal activity and optogenetic traces in awake mice,[15] such procedures typically require general anesthesia for proper clamp placement. These instruments often involve immobilizing the head, and some procedures are highly invasive, requiring pins to be set into the animal's skull.[16] Less invasive stereotaxic techniques for fluorescence optogenetic microscopy on awake and freely mobile mice have resulted in significant advances in the study of locomotion.[17, 18] In the clinical setting, wearable head mounts have recently been proposed for magnetoencephalography and stroke detection.[19, 20]

Minimally invasive stereotaxic techniques are also in demand for studies of the mouse eye. Commonly used anesthetics, such as ketamine-xylazine, are known to change the refractive index of the mouse eye,[21] and an animal under anesthesia needs external ocular moisturization.[22] In addition to stereotactic mounts,[23, 24] experimental techniques for ophthalmic imaging include conditioning animals for stability[22] and manually holding animals in place.[25] These techniques also require general anesthesia to restrict movement, but anesthesia can distort the physiology of the animal. Therefore, a stereotaxic mount that immobilizes imaging devices relative to the mouse eye would be very useful for mouse ophthalmology research. For example, the immune-privileged state of the eye facilitates engraftment of pancreatic beta cells in the anterior chamber of the mouse eye, which allows the eye to serve as a window for imaging the development of diabetes *in vivo*. Engraftment of these cells in the mouse eye has allowed noninvasive laser scanning microscopy of islet vascularization, beta-cell function, calcium dynamics,[26] measurement of *in vivo* glucose metabolism[27] and islet cell death at cellular resolution,[28, 29] leading to novel insights for the clinical treatment of diabetes.[30] These transplantation and imaging techniques for islet cells have depended on stereotaxic immobilization of the mouse head.[31]

In this article, we describe a system for stereotaxic imaging in awake and freely mobile mice that uses a head mount to immobilize optical probes relative to the mouse head. The head mount is fabricated using additive manufacturing (3D printing), and images are acquired via flexible micro-endoscopy probes. The head mount is customized to fit the specific age and size of the mouse under study using computed tomography (CT) scans, and the probe is immobilized relative to the mouse eye without breaking the skin or tympanic membrane and without need for anesthesia. The flexible endoscopy probe (1.0 mm in diameter) replaces the microscope-based imaging objective that is conventionally used to image the mouse eye.[32–34] This flexible probe allows long-term continuous imaging of the freely mobile mouse *in vivo* at cellular resolution (<20 μm) with a field of view of nearly 1 mm. The system is demonstrated by imaging the vasculature of the iris in mice injected with fluorescein isothiocyanate (FITC). The proposed head mount design can be adapted for other applications, such as *in situ* stimulation of the aural system of freely moving mice.

2 | MATERIALS AND METHODS

2.1 | System design

Imaging the eye of an awake and freely moving mouse requires the immobilization of imaging optics relative to the mouse head, an imaging system for reading out an image despite mouse movement, and an experimental design which allows freedom of movement to the mouse. As shown in Figure 1, these objectives are accomplished using a stereotaxic head mount system designed (Figure 1A) to immobilize in all three degrees of freedom with respect to the mouse head a flexible micro-endoscopy probe with gradient index (GRIN) imaging lenses, allowing for cellular resolution of the mouse eye (Figure 1B), and for the use of a confocal laser scanning microscopy platform for illumination and imaging (Figure 1C).

2.2 | 3D modeling of the mouse head

Computer-aided design (CAD) models of the mouse head, acquired using CT scans of an adult mouse, were used to build the stereotaxic head mount. A single adult female mouse was anesthetized following the protocols in the Section 2.5, and imaged using a Bruker SkyScan1176 CT device at 70 ms exposure with 2×2 binning, for a final axial resolution of 3 μm and a transverse pixel size of 35.76×35.76 μm. The resulting scanned projection radiography image (Figure 2A) shows most of the mouse body. A more detailed profile of the mouse head, including cranial structure, is shown in Figure 2B. Following binning and processing, 814 cross-sectional images of 608×608 pixels each were obtained. The cross-sections were segmented and formed
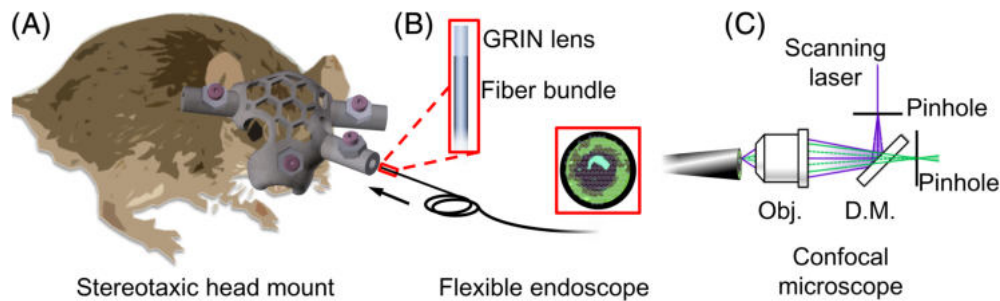
FIGURE 1 Schematic diagram of the stereotaxic helmet system used to image the vasculature of the iris. A, The stereotaxic head mount is placed on an alert, freely moving mouse. A flexible endoscope is inserted into an instrument channel on the head mount. B, The endoscopy probe consists of a GRIN imaging lens placed on the end of a coherent fiber bundle, allowing cellular-resolution imaging of the anterior segment of the mouse eye. C, A confocal laser scanning microscope is used to excite fluorophores in the eye vasculature, and the image is read out onto a photomultiplier tube detector. D.M., dichroic mirror; GRIN, gradient index; Obj., objective lens
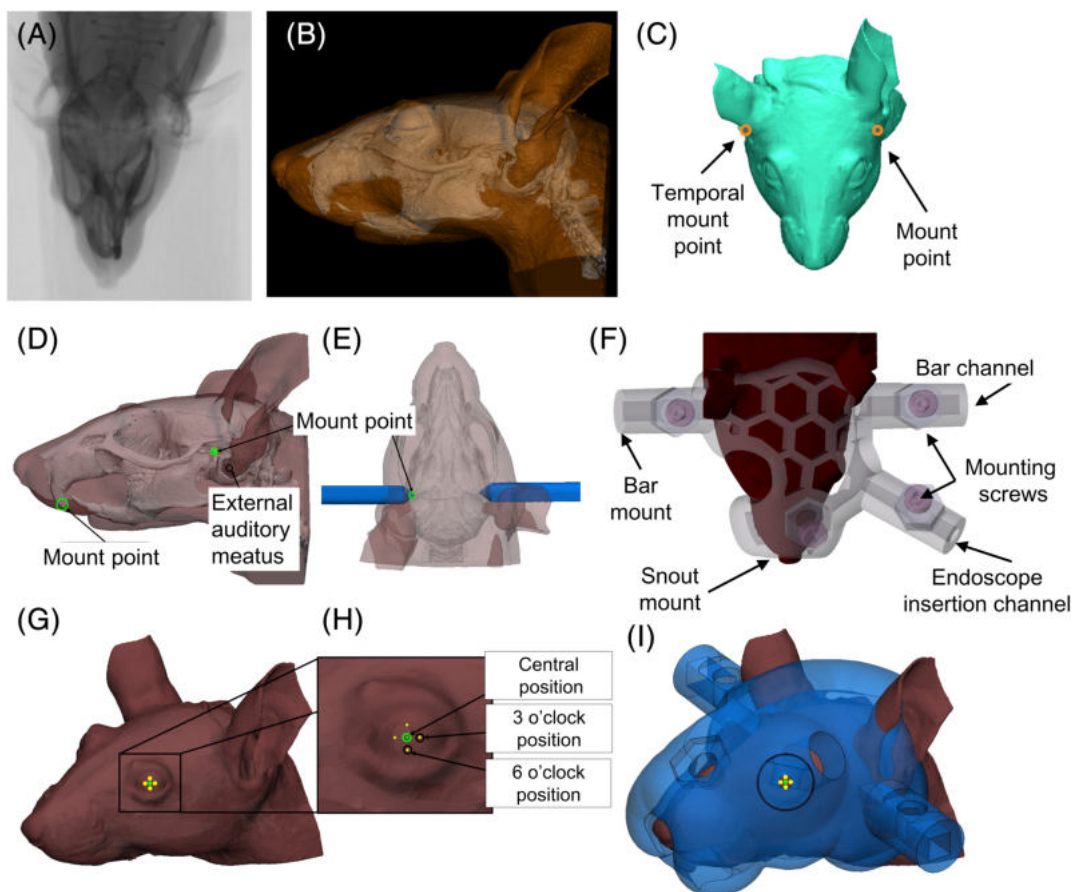

FIGURE 2 Design process for the stereotaxic head mount. A and B, Scanned projection radiography and 3D-rendered images of the mouse head and neck from computed tomography (CT) imaging were segmented and used to create C, a CAD model of the mouse head from which, C, D, E, suitable mount points were identified. F, Channels for bar mounts and incisor-type snout mounts were located, and instrument channels were designed into the head mount. G and H, Various insertion guide channels were designed around target points on the mouse eye. I, A simulated head mount design based around the identified mount point and target points

into a triangulated surface-based CAD model of the mouse head and cranium, as shown in Figure 2C,D, around which the head mount was designed. For visualization and testing, models were manufactured using 3D printing, as described in the Section 2.4.

2.3 | Design of the head mount

As the mouse is observed while awake and freely moving, the head mount must be securely mounted to the head with minimal trauma. Furthermore, the mounting

system must allow the mouse to breathe, while also guaranteeing stable access to the eye via an instrument channel. If anesthesia is used, experimental access to the mouth is also necessary. Stereotaxic clamping typically involves using incisor bars or palette and ear bars,[14] and care must be taken to ensure that these bars do not restrict the airway or break the tympanic membrane.[12, 35] The stereotaxic head mount attaches over the snout, with holes to fit the incisors into a bar which holds the mouth open (Figure S1), while ear bars fix to two points on the temporal lobes, roughly 2 mm in front of the ears. An additional bolt on the nose may be used to provide force to immobilize the incisor bar. The resulting three fixed points stabilize the head mount with respect to the mouse head while minimizing trauma and reducing slip. A CAD model of the mouse head was prepared by segmenting CT profiles, and the selected fixed points are shown in Figure 2C-E. Non-penetrating polymer temporal mount bars were inserted through square mounting holes (channels) in the head mount until they were snug around the mouse head, held in place by M3 setscrews, as shown in Figure 2F. The setscrews were designed to be threaded through nuts that were adhered to the holes in the bar mounts. The bar channels were 11 mm long, while the temporal mount bars were 18 mm long with $2 \text{ mm} \times 2 \text{ mm}$ rectangular cross-sections and pyramid-shaped tips.

For precise and repeatable access to the mouse eyes, the right eye was kept uncovered, and the endoscopy probe was immobilized using a circular instrument channel that is 15 mm in length and 1.5 mm in diameter. The instrument channel can be designed to be positioned either perpendicular to the center of the mouse eye or off-center at the 3 o'clock or 6 o'clock position, depending on the experiment design, as shown in Figure 2G,H. Devices with instrument channels positioned off-center by up to 30° were tested. Like the mounting channel, the instrument channel can incorporate a setscrew for precise placement of the instrument or imaging optic. An additional bolt on the nose may be used to finely adjust the positioning of the imaging optic vertically on the eye. The full design is shown in Figure 2F,I with a semitransparent model of the mouse head for clarity.

2.4 | Additive manufacturing and assembly

For convenience, low fabrication cost, precision and nontoxicity, stereotaxic head mount prototypes were printed by a stereolithographic 3D printer (SLA) with the clear polymer RS-F2-GPCL-04 (Formlabs Inc, Somerville, Massachusetts), as shown in Figure 3. Formlabs Clear Resin

provides high durability and stability. The 3D printer used for SLA was the Form2 (Formlabs), resulting in a transverse resolution of 150 μm, an axial resolution of 25 μm, and total printing time of 7 hours for 3 head mounts and 12 ear bars.

The final head mount prototypes had dimensions of roughly $45 \text{ mm} \times 31 \text{ mm} \times 23 \text{ mm}$, with printed parts having a volume of ~5.7 mL per head mount, including support structures of identical material. A few strategies for fixing the head mounts were attempted, including a strap (Figure S2A), temporal mount bars with holes for metal nuts and bolts (Figure S2B), and temporal mount bars with printed setscrews (Figure S2C). The strap proved insufficient to counter slipping, printed setscrews snapped easily while tightening, and metal screws added sufficient weight to prohibit free movement for some mice. Early models were printed using a multi-jet printing process on a 3D systems ProJet 3510SD printer. The final design, using lightweight temporal mount bars, and with a meshed structure to reduce the mount weight, is shown in Figure 3A-C and F-H. Lightweight polycarbonate bolts and nuts, 0.32 g total, were used for setting the ear bar and endoscope positions. The fully-assembled meshed head mount with setscrews and ear bars had a total mass of 2.54 g.

For demonstration of imaging channel angles prior to *in vivo* application, stereotaxic head mount prototypes were printed using two polymers from the Polyjet line of 3D printing materials, Vero and Agilus (Stratasys, Eden Prairie, Minnesota), on the Objet500 Connex3 printer, with a resolution of 30 μm, as shown in Figure 3D,E.

2.5 | Animal experiments

Animal experiments were performed according to protocols approved by the Institutional Animal Care and Use Committee (IACUC) of the ASAN Institute for Life Sciences, ASAN Medical Center (2019-12-261). The committee also followed the guidelines set by the Institute of Laboratory Animal Resources (ILAR), following the Laboratory Animal Act of the Republic of Korea.

2.6 | Computed tomography

For CT scanning, a single adult female mouse was anesthetized with a mixture of ketamine and xylazine anesthesia at a dose of 100 mg ketamine and 10 mg xylazine per kilogram body weight, given intraperitoneally.[35] This dose was sufficient to subdue the mouse for 10 to 15 minutes. CT images were captured with a 7 minutes exposure time.
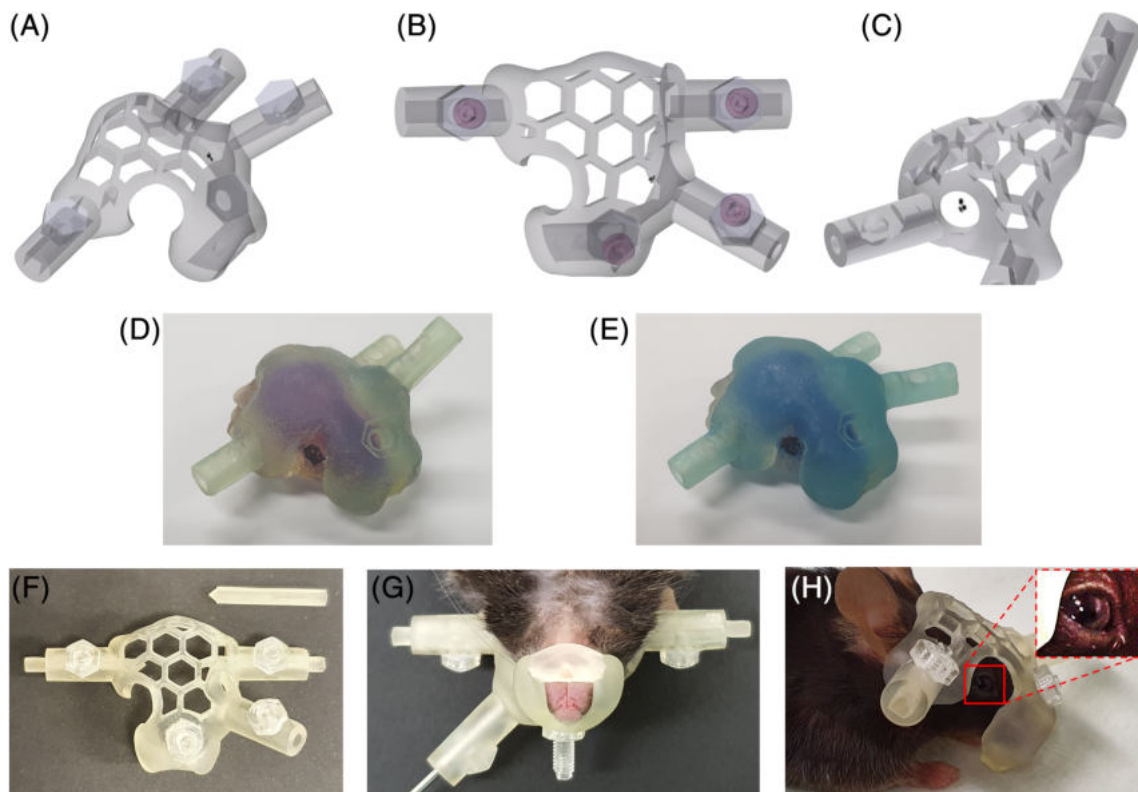
FIGURE 3 Instantiation of the stereotaxic head mount. A and B, Views of the head mount. C, Left-side view of the head mount, showing the center, 3 o'clock, and 6 o'clock points as black dots to demonstrate endoscope alignment through the left-side observation hole. D and E, Printed head mounts on printed mouse head phantoms, showing two different angles of instrument channels. F, The head mounts, as well as the mounting bars, were fabricated using additive manufacturing. G, The device is applied under anesthesia, showing the snout mount. H, The device is demonstrated on an awake and freely mobile mouse. (H, inset) A contrast-enhanced close-up of the mouse eye shows no orbital tightening, indicating minimal mouse pain

2.7 | Head mount testing and fitting procedure

After testing on a phantom mouse head, the head mount design was tested on a cohort of five adult mice with similar demographics to the adult female mouse used for CT scanning. Mice were anesthetized following established protocols with a mixture of 2.5% isoflurane (vol/vol) in 40% (vol/vol) O2 and 60% (vol/vol) N2 following Speier. [29] This subdued the mice for 10 to 15 minutes, during which time each mouse was placed on its back and the head mount was attached as shown in Figure 3G. Several tens of minutes after placement, the mice were comfortable in the devices, showing no signs of stress, and the temporal mount bars had a snug fit. A mouse is shown during the fitting process in Figure 3H (Supporting video).

2.8 | *In vivo* iris fluorescent angiography

No anesthetics were used to image the vascularization of the iris in active mice. FITC-dextran was dissolved in

sterile 5% (wt/vol) saline and filtered through a 0.45 μm syringe filter. Mice from the above cohort were intravenously injected with 0.1 mL of FITC-dextran in solution 20 minutes prior to imaging.

2.9 | Imaging setup and flexible coherent fiber bundle endoscope

While the head mount is compatible with a variety of optical probes, flexible coherent fiber bundle endoscopy probes were used because of their high resolution, ability to image at large physical depths and the ability of the probe to flex from the stationary optical probe mount to the freely moving animal. Recently, flexible fiber bundle probes with diameters as small as 350 μm have become commercially available, but for this application, which does not require surgical access, a millimeter-scale probe was sufficient. A fiber bundle of 30 000 imaging fibers was modified with a GRIN imaging lens to allow cellular-resolution imaging in the forward-facing imaging modality. Although in principle other lenses could be used,

GRIN lenses provide several benefits over conventional lenses for this application, including ease of lens alignment and a simplified housing assembly, narrower lens diameters, and working distances which can be varied by polishing on a planar surface. A GRIN lens (NA = 0.5) 1.00 mm in diameter and 2.05 mm in length (GRINTECH) with a working distance of 0.15 mm was adhered to the end of a coherent 30 000-fiber bundle with a diameter of 950 μm (Fujikura/Myriad), following previously published protocols.[36] The GRIN lens fiber bundle was inserted into a stainless-steel protective sleeve with a diameter of 1.25 mm and a length of 31 mm. The sleeve supports and protects the lens assembly from the force of the setscrew. The fiber bundle is shown schematically in Figure 4A and with a stainless-steel protective sleeve in Figure 4B. Despite a reduced field of view due to the GRIN lens, Figure 4C,D shows that the probe has uniform illumination with a resolution of 7.8 μm and a field of view of 928 μm, although image quality is observed to degrade toward the edge of the field of view (Figure 4D, E). The most suitable probe type can be selected for different experimental and imaging requirements.

2.10 | Laser scanning confocal microscope

A home-built confocal microscopy system was used with scanning laser illumination at 488 nm for excitation and imaging of the vasculature in the anterior chamber of the mouse eye. The fiber bundle was coupled via an infinity-corrected objective lens (NA 0.4, 20x, Zeiss) and focused on the proximal endoscope probe tip so that the image of the endoscope probe tip matched the dimensions of the camera sensor and illumination source. A 488 nm scanning laser was used to excite FITC-dextran and GFP in the target animal. The fluorescent image passed through a 525 nm cut-off long-pass filter to remove scattered and reflected illumination before photomultiplier tube detector imaging. Due to the fiber bundle in the probe, neither depth-based imaging nor assessment of axial focal distance was performed.

2.11 | Image post-processing and statistics

Collected images were balanced for increased contrast following the application of a Gaussian long-pass filter to remove the pixilation and moiré patterns that emerge due to an imperfect match between the hexagonal pattern of the fiber bundle and the detector sampling. In areas where the number of photons collected was very small, the contrast of the resulted images was renormalized. Five images were captured using identical USAF targets and endoscopes for reporting of endoscope resolution. Performance was observed to vary by at most two elements on the USAF test chart. The reported resolution is the mean of these measurements. For tissue paper and *in vivo* images, the measured resolution is the diameter of the smallest distinguishable fiber or blood vessel in the image, as calculated using the FOV size from the USAF test chart. The mean of N = 5 images is reported.

3 | RESULTS AND DISCUSSION

Practical imaging of the eye of an awake and freely moving mouse requires calibrated imaging optics, immobilization of the head mount and probe relative to the mouse head,
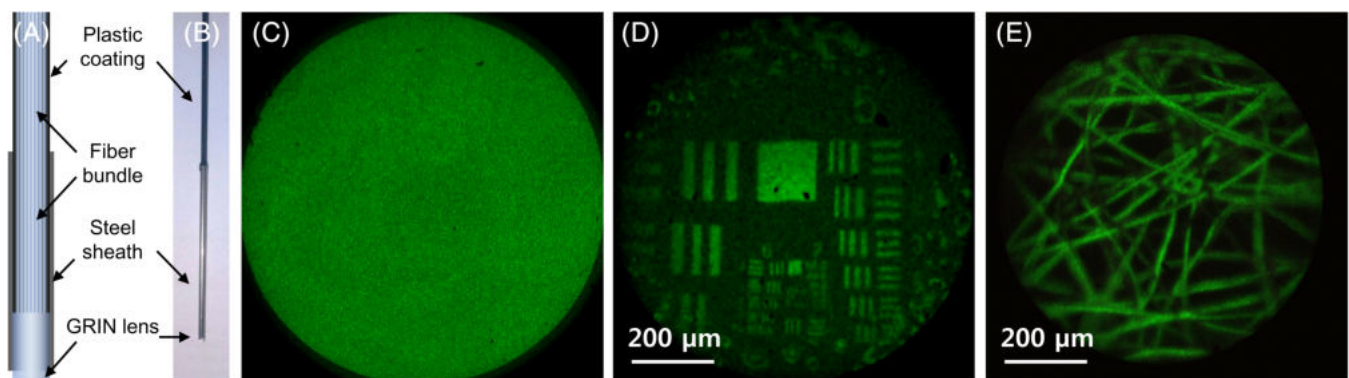

FIGURE 4 A, Schematic of the endoscope probe consisting of a GRIN lens mounted on a flexible coherent fiber bundle, which enables cellular-resolution imaging of the mouse eye. B, Photograph of the same endoscope probe with a protective stainless-steel sleeve. C, End facet of the endoscope probe under uniform illumination confirms minimal dirt and uniform illumination before measurement. D, Image of a USAF 1951 target shows that the field of view of the micro-endoscope is ~928 μm in air. E, Imaging of lens cleaning tissue demonstrating that fibers as small as 20 μm are clearly resolved. Scale bars, 200 μm. GRIN, gradient index

and the capability for both visual and fluorescence imaging. Stand-alone endoscopy probes were tested with the confocal scanning laser illumination and imaging system before being used in animal experiments. The head mount itself was tested for animal comfort, and vasculature imaging was demonstrated.

3.1 | Performance of the endoscope probe

Before biological imaging, the performance of the stand-alone endoscope probes in the complete optical system was confirmed by connecting the endoscopes to the Leica scanning microscope via the mounting system. Endoscope probe in air tests with defocused targets (shown in Figure 4C) reveal a Gaussian illumination intensity distribution with a mean of 110.8 and a SD of 15.5, for a full width at half maximum (FWHM) of 37, or 33%. A USAF 1951 resolution target was imaged to determine the transverse resolution and field of view (Figure 4D), and the smallest lines of a USAF 1951 resolution target that are fully resolved are in group 6, element 2. Across five samplings, the mean resolution corresponded to 64 line-pairs per millimeter (lp/mm) and a resolution of ~7.8 μm. The field of view is 928 μm. Lens paper with ~20 μm minimum thread size, as calculated from the imaging scale, was imaged as a proof of concept (in Figure 4E). Post-processing with Gaussian filtering and increased contrast resulted in slightly higher image quality.

3.2 | Head mount stability, attachment and noninvasiveness

The stereotaxic head mount was designed based on CT images of an adult mouse head to have maximum stability with minimal discomfort and injury risk in an awake and freely moving mouse. A polymer phantom model was manufactured by additive manufacturing and used to test the mounting on the mural cranium.

When designing a new experimental animal model imaging modality, it is necessary to test the comfort of the experimental animals. Following ethical best practices, the comfort of the ear bar and nose mount systems was evaluated in awake, freely moving mice *in vivo*. The mouse grimace scale (MGS)[37] was used to determine the pain level pain and discomfort of mice while mounting the device. No discomfort was exhibited by the mice before the mounting of the temporal mount bars, as shown in Figure 3H. As the bars were tightened, the mice expressed small amounts of discomfort, ranging from 0 to 1 in the orbital tightening and ear position metrics of the

MGS, and remained at 0 for the check bulge metric. Nose bulge and whisker change could not be assessed due to the design of the head mount.

Alignment of the imaging probe to the mouse eye required a fitting procedure. As the 3D-printed nature of the device does not allow for *in situ* modification of the imaging channel, careful placement of the ear bars is necessary for adjustment of the imaging position. A hole in the left side of the mount (Figure 3C) can be used to track the position of the imaging probe relative to the eye. For fine adjustment, a flat-tipped bolt may be added to lift the head mount off the nose.

3.3 | *In vivo* iris fluorescence angiography

The efficacy of the stereotaxic head mount for live monitoring of awake and alert animals was demonstrated using a forward-facing GRIN endoscope assembly at the end of a flexible coherent fiber bundle probe. At an illumination wavelength of 488 nm and an imaging wavelength of 525 nm, a penetration depth of 2.5 mm into brain tissue can be achieved[38]; however, the mouse eye is nearly transparent at these wavelengths. Images of the mouse eye were first obtained using standard photographic equipment show the target location of the eye, as shown in Figure 5A, before micro-endoscopic imaging was performed. The eye vasculature in live animals was imaged after injection of FITC-dextran. The resultant vasculature images are shown in Figure 5B. Vessels as narrow as 20 μm and larger blood vessels up to 800 μm in length are visible against the defocused ocular background. The images attained would be suitable for studying ocular diseases of the anterior chamber and their treatments, such as iritis, Axenfeld-Rieger syndrome, iridocorneal endothelial syndrome, pigment dispersion syndrome, Rieger's anomaly, Peter's anomaly and megalocornea, where mouse models are available.

3.4 | Limitations and potential improvements

The present implementation of the head mount for mice has several notable limitations. In particular, geometric imaging parameters are constrained during fabrication of the head mount. Although this first implementation of the head mount device required a CT scan of an individual mouse for fitting on a cohort of similarly sized mice, it is anticipated that the present design may be modified for additional cohorts of mice once adjustments are made for any discrepancies in the distance from the mouse snout to the eyes and to the ear bars, and to a lesser
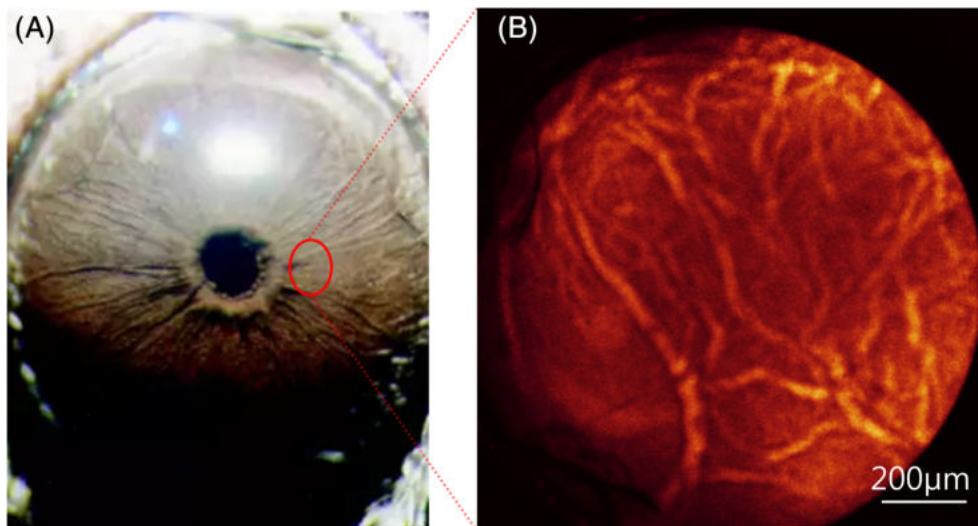
FIGURE 5 Images obtained from the stereotaxic endoscopic imaging system of awake and alert mice demonstrate system utility. A, Photographic images of the mouse eye before head mount fitting. B, Fluorescent micro-endoscopic image of the corresponding eye showing iris vasculature in the 3 o'clock position of the mouse iris using FITC-dextran. Scale bars are 200 μm. FITC, fluorescein isothiocyanate

extent in the width of the mouse head and the intraocular distance. Furthermore, while the initial CT scan is expensive, the unit cost of fabrication can be divided over the size of each similarly sized mouse cohort.

Although the present design is limited, in that adjusting the angle of the imaging channel requires changing mounts, future designs of the head mount may incorporate multiple imaging channels at different angles or position the channel on a ball joint. At present, these features have been omitted to reduce device weight and complexity.

The applicability of the head mount depends significantly on the capabilities of the associated endoscopic imaging platform. With the ongoing development of microprobes suitable for angiographic optical coherence tomography,[39, 40] photoacoustic microscopy for retinal diagnosis[41, 42] and diagnosis based on deep learning,[43, 44] the stereotaxic head mount promises extensibility for the future of micro-endoscopic animal studies of eye disease.

4 | CONCLUSION

This study evaluates the use of a stereotaxic head mount for the imaging of the mouse eye in awake and freely moving mice. The mount is designed for minimal invasiveness and ease of use and is fabricated using additive manufacturing. Preliminary experiments clearly demonstrate the ability of the system to perform *in vivo* imaging, including single-cell imaging, optical biopsy and tumor progression studies in small-animal models. Front-view flexible endoscopy probes provide imaging at a resolution of 7.8 μm, with a field of view of 928 μm. *in vivo* images capture features of iris vasculature in the mouse as small as 20 μm in size. This head mount design is of particular utility for low-cost small-animal stereotaxic

experimentation, where noninvasive optical imaging techniques are in high demand and will be particularly useful for researchers with experience in stereotaxic techniques who would like to extend their existing research in awake, freely moving animals. The system concept can be extended for fast prototyping of small-animal experiments, both stereotaxic and non-stereotaxic, as will be required for the next generation of preclinical animal studies. In conclusion, the development of the stereotaxic head mount system, with its 3D-printed assembly and practical imaging modalities, paves the way toward low-cost confocal micro-endoscopic imaging modalities in small-animal disease models.

CONFLICT OF INTEREST
The authors declare no financial or commercial conflict of interest.

AUTHOR CONTRIBUTIONS
B.P., S.L. were involved in investigation, writing-original draft, review, and editing. K.L. and M.J. were involved in animal experiment design and implementation. S.L., G.B.K., Y.M., J.Y.L., and were involved in advising,

review, and editing. N.K. and J.K.K. were involved in conceptualization, experiment design, and project management. J.K.K was also writing, review, editing, supervising, and financial supporting.

REFERENCES

[1] E. J. Nestler, S. E. Hyman, *Nat. Neurosci.* **2010**, *13*, 1161.
[2] S. Lesné, M. T. Koh, L. Kotilinek, R. Kayed, C. G. Glabe, A. Yang, M. Gallagher, K. H. Ashe, *Nature* **2006**, *440*, 352.
[3] J. L. Silverman, M. Yang, C. Lord, J. N. Crawley, *Nat. Rev. Neurosci.* **2010**, *11*, 490.
[4] K. M. Tye, K. Deisseroth, *Nat. Rev. Neurosci.* **2012**, *13*, 251.
[5] L. Fenno, O. Yizhar, K. Deisseroth, *Annu. Rev. Neurosci.* **2011**, *34*, 389.
[6] L. M. Chalupa, R. W. Williams Eds., *Eye, Retina, and Visual System of the Mouse*, MIT Press, Cambridge, MA **2008**.
[7] Z. J. Huang, A. Kirkwood, T. Pizzorusso, V. Porciatti, B. Morales, M. F. Bear, L. Maffei, S. Tonegawa, *Cell* **1999**, *98*, 739.
[8] C. M. Niell, M. P. Stryker, *J. Neurosci.* **2008**, *28*, 7520.
[9] T. L. Van Belle, P. Taylor, M. G. von Herrath, *Models* **2009**, *6*, 41.
[10] A. J. King, *Br. J. Pharmacol.* **2012**, *166*, 877.
[11] G. Paxinos, K. B. J. Franklin, *Paxinos and Franklin's the Mouse Brain in Stereotaxic Coordinates*, Academic Press, Cambridge **2019**.
[12] C. Messier, S. Émond, K. Ethier, *Pharmacol. Biochem. Behav.* **1999**, *63*, 313.
[13] B. M. Slotnick, *Physiol. Behav.* **1972**, *8*, 139.
[14] *Current Protocols in Neuroscience* (Eds: J. N. Crawley, C. R. Gerfen, M. A. Rogawski, D. R. Sibley, P. Skolnick, S. Wray), John Wiley & Sons, Inc., Hoboken, NJ **2005**.
[15] J. L. Bryant, S. Roy, D. H. Heck, *J. Neurosci. Methods* **2009**, *178*, 75.
[16] M. R. Hodges, G. J. Tattersall, M. B. Harris, S. D. McEvoy, D. N. Richerson, E. S. Deneris, R. L. Johnson, Z.-F. Chen, G. B. Richerson, *J. Neurosci.* **2008**, *28*, 2495.
[17] F. Helmchen, M. S. Fee, D. W. Tank, W. Denk, *Neuron* **2001**, *31*, 903.
[18] K. K. Ghosh, L. D. Burns, E. D. Cocker, A. Nimmerjahn, Y. Ziv, A. E. Gamal, M. J. Schnitzer, *Nat. Methods* **2011**, *8*, 871.
[19] E. Boto, N. Holmes, J. Leggett, G. Roberts, V. Shah, S. S. Meyer, L. D. Muñoz, K. J. Mullinger, T. M. Tierney, S. Bestmann, G. R. Barnes, R. Bowtell, M. J. Brookes, *Nature* **2018**, *555*, 657.
[20] J. Griffith, K. Cluff, B. Eckerman, J. Aldrich, R. Becker, P. Moore-Jansen, J. Patterson, *Sensors.* **2018**, *18*, 1022.
[21] T. V. Tkatchenko, A. V. Tkatchenko, *J. Neurosci. Methods* **2010**, *193*, 67.
[22] E. G. de la Cera, G. Rodríguez, L. Llorente, F. Schaeffel, S. Marcos, *Vision Res.* **2006**, *46*, 2546.
[23] H. A. Reitsamer, J. W. Kiel, J. M. Harrison, N. L. Ransom, S. J. McKinnon, *Exp. Eye Res.* **2004**, *78*, 799.
[24] T. V. Tkatchenko, Y. Shen, A. V. Tkatchenko, *Invest. Ophthalmol. Vis. Sci.* **2010**, *51*, 21.
[25] N. L. Hawes, R. S. Smith, B. Chang, M. Davisson, J. R. Heckenlively, S. W. John, *Mol. Vis.* **1999**, *5*, 22.
[26] C. Chen, H. Chmelova, C. M. Cohrs, J. A. Chouinard, S. R. Jahn, J. Stertmann, I. Uphues, S. Speier, *Diabetes* **2016**, *65*, 2676.
[27] G. Li, B. Wu, M. G. Ward, A. C. N. Chong, S. Mukherjee, S. Chen, M. Hao, *J. Cell Sci.* **2016**, *129*, 2865.
[28] S. Speier, D. Nyqvist, O. Cabrera, J. Yu, R. D. Molano, A. Pileggi, T. Moede, M. Köhler, J. Wilbertz, B. Leibiger, C. Ricordi, I. B. Leibiger, A. Caicedo, P. O. Berggren, *Nat. Med.* **2008**, *14*, 574.
[29] S. Speier, D. Nyqvist, M. Köhler, A. Caicedo, I. B. Leibiger, P.-O. Berggren, *Nat. Protoc.* **2008**, *3*, 1278.
[30] M. H. Abdulreda, R. Rodriguez-Diaz, A. Caicedo, P.-O. Berggren, *Cell Metab.* **2016**, *23*, 541.
[31] M. H. Abdulreda, A. Caicedo, P.-O. Berggren, *Regen. Reprogramming.* **2013**, *1*, 111.
[32] J. Kim, J. R. Park, J. Choi, I. Park, Y. Hwang, H. Bae, Y. Kim, W. Choi, J. M. Yang, S. Han, T. Y. Chung, P. Kim, Y. Kubota, H. G. Augustin, W. Y. Oh, G. Y. Koh, *Sci. Adv.* **2019**, *5*, 6732.
[33] J. R. Park, W. Choi, H. K. Hong, Y. Kim, S. Jun Park, Y. Hwang, P. Kim, S. Joon Woo, K. Hyung Park, W.-Y. O., *Investig. Opthalmol. Vis. Sci.* **2016**, *57*, OCT331.
[34] J. Y. Lee, Y. Hwang, J. H. Kim, Y. S. Kim, B. K. Jung, P. Kim, H. Lee, *Investig. Opthalmol. Vis. Sci.* **2016**, *57*, 3390.
[35] A. Cetin, S. Komai, M. Eliava, P. H. Seeburg, P. Osten, *Nat. Protoc.* **2007**, *1*, 3166.
[36] J. K. Kim, W. M. Lee, P. Kim, M. Choi, K. Jung, S. Kim, S. H. Yun, *Nat. Protoc.* **2012**, *7*, 1456.
[37] D. J. Langford, A. L. Bailey, M. L. Chanda, S. E. Clarke, T. E. Drummond, S. Echols, S. Glick, J. Ingrao, T. Klassen-Ross, M. L. LaCroix-Fralish, L. Matsumiya, R. E. Sorge, S. G. Sotocinal, J. M. Tabaka, D. Wong, A. M. J. M. van den Maagdenberg, M. D. Ferrari, K. D. Craig, J. S. Mogil, *Nat. Methods* **2010**, *7*, 447.
[38] S. K. Powers, J. T. Brown, *Lasers Surg. Med.* **1986**, *6*, 318.
[39] W. J. Choi, *Biomed. Eng. Lett.* **2019**, *9*, 311.
[40] H. Makhlouf, A. R. Rouse, A. F. Gmitro, *Opt. Express* **2011**, *2*, 634.
[41] W. Liu, J. Yao, *Biomed. Eng. Lett.* **2018**, *8*, 203.
[42] P. Hajireza, W. Shi, R. J. Zemp, *Opt. Lett.* **2011**, *36*, 4107.
[43] R. F. Mansour, *Biomed. Eng. Lett.* **2018**, *8*, 41.
[44] Y. Tang, A. D. Polydorides, S. Anandasabapathy, R. R. Richards-Kortum, *J. Biomed. Opt.* **2018**, *23*, 1.

SUPPORTING INFORMATION
Additional supporting information may be found online in the Supporting Information section at the end of this article.